Wet-spun porous carbon microfibers for enhanced electrochemical detection

Journal:	*ACS Applied Materials & Interfaces*
Manuscript ID	am-2023-00423s.R1
Manuscript Type:	Article
Date Submitted by the Author:	13-Mar-2023
Complete List of Authors:	Ostertag, Blaise; University of Cincinnati, Chemistry Ross, Ashley; University of Cincinnati, Chemistry

Wet-spun porous carbon microfibers for enhanced electrochemical detection

Blaise Ostertag[1] and Ashley E. Ross[1,*]

[1]University of Cincinnati
Department of Chemistry
312 College Dr.
404 Crosley Tower
Cincinnati, OH 45221-0172, USA

Office Phone#: 513-556-9314
Email: Ashley.ross@uc.edu

*Corresponding author

ORCID

Blaise J. Ostertag 0000-0003-4970-9742

Ashley E. Ross 0000-0003-2456-3636

Keywords: porous carbon, electrochemistry, sensors, voltammetry, wetspinning, copolymers

Abstract

We present a novel copolymer-based, uniform porous carbon microfiber (PCMF) formed via wet-spinning for significantly improved electrochemical detection. Carbon fiber (CF), fabricated from a polyacrylonitrile (PAN) precursor, is commonly used in batteries or for electrochemical detection of neurochemicals due to its bi-planar geometry and desirable edge plane sites with high surface free energy and defects for enhanced analyte interactions. Recently, the presence of pores within carbon materials has presented interesting electrochemistry leading to detection improvements; however, there is currently no method to uniformly create pores on a a carbon microfiber surface impacting a broad range of electrochemical applications. Here, we synthesized controllable porous carbon fibers from a spinning dope of the copolymers PAN and polymethyl methacrylate (PMMA) in dimethylformamide via wet spinning for the first time. PMMA serves as a sacrificial block introducing macropores of increased edge-plane character on the fiber. Methods were optimized to produce porous CFs at similar dimensions to traditional CF. We prove that an increase in porosity enhances the degree of disorder on the surface, resulting in significantly improved detection capabilities with fast-scan cyclic voltammetry. Local trapping of analytes at porous geometries enables redox cycling with improved sensitivity, linear range of detection, and measurement temporal resolution. Overall, we demonstrate the utility of a copolymer synthetic method for PCMF fabrication, providing a stable, controlled macroporous fiber framework with enhanced edge plane character. This work will significantly advance fundamental investigations of how pores and edge plane sites influence electrochemical detection.

Introduction

Real-time neurotransmitter detection has been dominated by lowly sensitive carbon-fiber microelectrodes (CFME) for decades;[1,2] but, here, we present a synthetic route to revolutionize the chemical and morphological structure of carbon microfibers (CF) for significantly improved detection capabilities. Specialized electrochemical methods using carbon-based materials have moved to the forefront as implantable biosensors. Foundational reports have characterized the importance of carbon edge-plane character for improved adsorption and electron transfer kinetics due to the increase in functionalized defects.[3,4] CF is traditionally amorphous which results in little control over the chemical structure of the material. This leads to non-uniform distribution of edge-plane character across the surface which can limit their wide-spread use as sensitive electrode materials. Porous geometries on electrode surfaces have proven redox enhancement properties; however, it is currently not possible to create uniform porosities on carbon-fiber microelectrodes which has also hindered wide-spread use of porous sensor surfaces for neurochemical detection.[5,6] Here, we developed a method to wet-spin porous carbon microfibers for the first time to fill this gap. This work was inspired by prior studies using sacrificial block-copolymer electrospinning approaches.[7–9] Our porous carbon microfibers permit local neurotransmitter trapping at the surface resulting in enhanced sensitivity, extended linear working regions, and significantly improved temporal resolution capabilities. To date, materials synthesized with these properties have yet to explore macro-scale porous framework properties since larger pore sizes negate sought after nanoscale catalytic properties and surface area increases for ion exchange in battery energy storage.[7,10] Prior approaches to synthesize porous carbon fibers have produced nanofiber mats through electrospinning,[11–13] which inhibits their use as microfiber sensors for biological detection. Additionally, mats of nanofibers are brittle and difficult to handle.[13] Overall, the work presented here presents a brand new carbon material for electrochemistry.

Dual-diffusion wetspinning of polyacrylonitrile (PAN) has monopolized CF production due to quick pyrolyzing processes for micron fiber diameter uniformity and post-treatment processing

for mechanical property enhancements with high carbon yields.[14] By introducing a secondary decomposing polymer, polymethyl-methacrylate (PMMA), pore formation is evident proceeding pyrolysis and annealing, and have uniform mesopore sizes that are highly controllable when using block-copolymerization. This block copolymerization phenomena has been vastly explored[15] in the supercapacitor realm[7–11] for specific surface area and electrocatalytic behavior, but electrochemistry explorations have found these geometries incompatible for redox enhancements from local analyte trapping.[6,16] Wetspinning, on the other hand, produces dimensionally compatible carbon microfibers of a continuous length for viable microelectrode fabrication applications for beneficial biosensing and can avoid fiber collapse, void formation, and extended surface defects,[17] with tunable geometries and tensile properties.[18] Although wetspinning is a widely accepted fiber spinning technique, few reports have explored porous microfiber formations, and of those that have, methods are still lacking for controlling pore geometry/distribution and surface morphology for enhanced analyte interactions rather than just internal porosity.[19] PAN-spinning dope additives could hold the key to maximizing mechanical properties[20,21] and, here, we show that doping additives enables an increase in defect sites and edge plane character accompanied by morphological advantages for increased analyte-electrode surface interactions.

Reformulating CF precursor spinning dopes with copolymer mixtures provide a means for uniform macropore formation of dimensional geometries compatible for creating multiple local thin-layer cell environments for momentary analyte trapping. To date, roughened geometries on carbon nanomaterials have been explored for kinetic improvements and thin-layer cell type characteristics for real-time neurochemical detection with fast-scan cyclic voltammetry (FSCV),[5,6,22] but their pore size and coverage remain difficult to control. Although uniform and controllable porosity still remains difficult with electrode materials used for FSCV, prior studies have demonstrated that pores and surface roughness increases result in local trapping of neurochemical analytes at the electrode's surface to enhance redox cycling, improve temporal resolution capabilities, and provide faster electron transfer kinetics. No current method exists for

controlling pore abundance, size, and distribution in microelectrode frameworks. This gap in approaches has limited our ability to fundamentally investigate precisely how pore size impacts electrochemical detection. We believe our method unlocks the capability of tuning carbon microfiber surface morphology and surface chemistry for enhanced biosensing applications. We show here that optimizing copolymer compositions enables maximizing the desirable edge plane electrochemistry and more pore uniformity not only for well-established catecholamine detection but other classes of neurotransmitters. Our results revolutionize the way we understand pore geometry and edge plane character impacts on real-time neurotransmitter detection. The results presented here also raise the question of whether the waveform application frequency independence and redox cycling behavior observed with carbon nanomaterials with FSCV is solely due to pore presence, or is some of it driven by surface interactions of desorbing molecules with abundant edge plane site enhancements?

Experimental Methods

Reagents

Precursor solution dope preparation consisted of mixing polyacrylonitrile (PAN – average MW = 150,000), poly(methyl methacrylate) (PMMA – average MW = 350,000), and N,N-Dimethylformamide ≥ 99.8% (DMF) all purchased from Sigma Aldrich (St. Louis, MO, USA). Wet-spinning coagulation and washing baths consisted of diluted DMF using Milli-Q deionized water (MilliporeSigma, Burlington, MA, USA). For electrochemical analysis, the chemical reagents potassium hydroxide (KOH), hydrochloric acid (HCl), and dopamine (DA) were purchased from Thermo Fisher Scientific (Waltham, MA, USA). 10 mM DA stock solutions were stored at 4°C after dissolving solid DA in 0.1 M HCl. Tris buffer (pH = 7.40) was used to dilute the stock solution to derive working solutions for experimentation. Tris buffer is prepared in Milli-Q deionized water consisting of 15 mM Tris Base, 140 mM NaCl, 3.25 mM KCl, 1.25 mM NaH_2PO_4 monohydrate,

1.20 mM $MgCl_2$ hexahydrate, 2 mM Na_2SO_4 anhydrous, and 1.20 mM $CaCl_2$ dihydrate all purchased from Thermo Fisher Scientific.

In-house wetting spinning apparatus specifications

An in-house wet-spinning setup was constructed from a 4" x 1" x 8' strip board (Home Depot, Atlanta, GA, USA) which was cut into two 32" and two 8.5" pieces creating a wet-spinning apparatus (see Supplemental Movie 1). Following apparatus construction, five 320 mm stainless steel threaded rods were fitted and centered with one ABEC-11 skateboard wheel bearing respectively for minimal friction (Amazon, Seattle, WA, USA) and placed horizontally across the apparatus. Two of these rods are set over the coagulation and washing baths respectively, each 4" apart with one rod in the center of the apparatus 3.5" from each bath rod and 0.25" higher to provide stretching and a transfer wheel for the precursor fiber from bath to bath with a 4.1° incline. This incline allows for stretching and alignment while not overcoming the maximum break stress of the precursor. The constructed apparatus was then placed on top of two 7" x 5" x 1.5" Pyrex containers to hold the coagulation and washing bath (Rosemont, IL, USA).

Copolymer solution preparation and precursor wet-spinning procedure

Coagulation bath solutions were diluted to a concentration of 79/21 DMF/Milli-Q H_2O and washing baths were diluted to a concentration of 20/80 DMF/Milli-Q H_2O. Mixed copolymer solutions dissolved in DMF were prepared at a total polymer concentration of 20% w/w and the ratio of the copolymers PAN and PMMA were varied from 95/5 to 70/30 PAN/PMMA. Solutions were then placed onto an Isotemp electric stirrer/hot plate from Thermo Fisher Scientific (Waltham, MA, USA) and stirred at 60°C for two hours at 100 rpm until all polymer dissolved (any undissolved polymer was filtered out of the solution). Copolymer solutions were then loaded into a 10 mL BD plastic syringe (Franklin Lakes, NJ, USA) fitted with a PTFE tubing kit from ramé-hart instrument co. (Succasunna, NJ, USA) and a Hamilton 90531 31-gauge needle with the needle stripped from the base to reduce resistance (La Vista, NE, USA). The syringe was then placed on

a Fusion 100 Two-Channel Syringe Pump (Chemyx Inc., Stafford, TX, USA) and the needle stub was clamped horizontally in the coagulation bath with the PTFE tubing filled at a flow rate of 3 mL min^{-1} until the solution filled the tubing and needle. The flow rate was then changed to 0.1 mL min^{-1} and the extruded precursor fiber was pulled by hand over and under wheel ball bearings, above the center transfer bearing and down into the washing bath (See Supplemental Movie 1). After pulling through the washing bath, the precursor fiber was pulled upward to collect using a DLS Digital Overhead Stirrer turned sideways (VELP Scientifica, Deer Park, NY, USA). A quartz rod (QSI Quartz Scientific, Fairport Harbor, OH, USA) spinning at 100 rpm collected the precursor fiber and provided additional stretching of the plasticized fiber as further extruded fiber was pulled through the wet-spinning apparatus. Following precursor fiber collection, precursors were dipped in Milli-Q H_2O to remove all solvent and wrapped around glass microscope slides to maintain tension and further stretching as the precursor dried in air. Once dried, precursor fibers were cut to a length of 4 cm and prepared for heating.

Carbonization and annealing of porous carbon fiber

Fully dried precursor PAN/PMMA fibers were loaded into a quartz sample holder and placed into a quartz process tube (QSI Quartz Scientific, Fairport Harbor, OH, USA) for heating in a tube furnace (Lindberg Blue M, Thermo Fisher Scientific, Asheville, NC, USA). Precursor fibers were heated for carbonization at 280°C for 5-hours resulting in air-oxidation rearranging the fiber's atomic bonding pattern from a linear to a ladder structure permitting further complex chemical reactions. Then, the gas cylinder-fitted process tube began N_2 gas flow for 15 minutes connected to a bubbler to ensure no back flow of air before temperature ramping for an inert atmosphere (Wright Brothers Inc., Cincinnati, OH, USA). Then, the temperature was ramped for pyrolysis, annealing, and finalization of PMMA decomposition to 1000°C at a rate of 15°C min^{-1}. This last step expels non-carbonaceous atoms in the form of various gases creating a tightly bonded carbon crystalline fiber.

Surface characterization

Chemical and physical properties of the copolymer-derived porous carbon fibers were analyzed using standard surface characterization techniques. Porous carbon fiber diameters, pore width measurements, and assessing and visualizing pore structures and their uniformity was performed using ImageJ 1.53k Java 1.8.0_172 (National Institutes of Health, USA) and scanning electron microscopy (SEM) using a FEI XL30 SEM at a 5.00 kV accelerating voltage. Pore depth and broadness measurements were made using atomic force microscopy (AFM) in non-contact tapping mode at a frequency of 1 Hz and 512 x 512-pixel resolution (Bruker Dimension Icon ScanAsyst AFM, Billerica, MA, USA). Tensile strength measurements were made using a 100N250-10 100 Series frame and actuator assembly from TestResources (Shakopee, MN, USA) with a Newton controller atop a PWA090 electronic, self-levelling, benchtop isolation system from ThorLabs (Newton, NJ, USA). Surface free energy measurements were investigated using a Sigma 700 Force Tensiometer from Biolin Scientific (Stockholm, Sweden) using a 70 mm vessel with Milli-Q H_2O and immersing carbon fibers at a depth of 2.5 mm. Raman spectra maps were collected using a Renishaw InVia Raman microscope (Guocestershire, UK) with an Ar-ion laser at a wavelength of 633 nm and a laser power of 10%.

PCMF microelectrode fabrication

75/25 PAN/PMMA porous carbon fibers (PCMFs) were fabricated into cylindrical microelectrodes for electrochemical analysis. Due to weaker mechanical properties, empty 1.2 mm x 0.68 mm x 4” glass capillary tubes (A-M Systems, Sequium, WA) were pulled vertically with an electrode puller (PE-22, Narishige Scientific, Tokyo, Japan) and the tip was scored back with a ceramic tile (Sutter Instrument Company, Novato, CA, USA) to expand the opening. Porous carbon microfibers (PCMFs) were then fed through the back opening of the pulled capillary tube and pushed up through the scored opening using a tungsten rod and sealed using an EPON Resin 828 liquid epoxy resin (Carson, CA, USA) mixed with m-Phenylenediamine (Acros Organics, NJ, USA). After the epoxy dried, PCMF microelectrodes were cut by hand to ~50 μm

for analysis. Electrodes were soaked in isopropyl alcohol for approximately 10 minutes prior to use to clean the surface.

Electrochemical characterization

A WaveNeuro potentiostat with a 1 MΩ headstage (Pine Instruments, Durham, NC, USA) was used to collect fast-scan cyclic voltammograms for electrochemical characterization with HDCV Software (UNC-Chapel Hill, Mark Wightman) and a National Instruments PC1e-6363 computer interface board (Austin, TX, USA). PCMF microelectrodes scanned from a -0.4 V holding potential to a 1.3 V switching potential and back *vs.* a Ag/AgCl reference electrode at a scan rate of 400 V s^{-1} and frequency of 10 Hz. Capacitive current was removed by background subtraction leaving only faradaic current plotted in the cyclic voltammogram (CV). Flow injection analysis was used for all microelectrodes to introduce analyte to the electrode surface using a Fusion 100 Two-Channel Syringe Pump (Chemyx, Stafford, TX, USA) and a flow rate of 1 mL min^{-1}.

Statistics

GraphPad Prism V. 9.0 (GraphPad Software Inc., La Jolla, CA, USA) was used to perform statistics with statistical p-values found to be significant at a 95% confidence interval. All values are reported as mean ± standard error of the mean (SEM) with electrode number denoted by *n*.

Results and Discussion

Porous carbon microfiber synthesis from PAN/PMMA copolymers

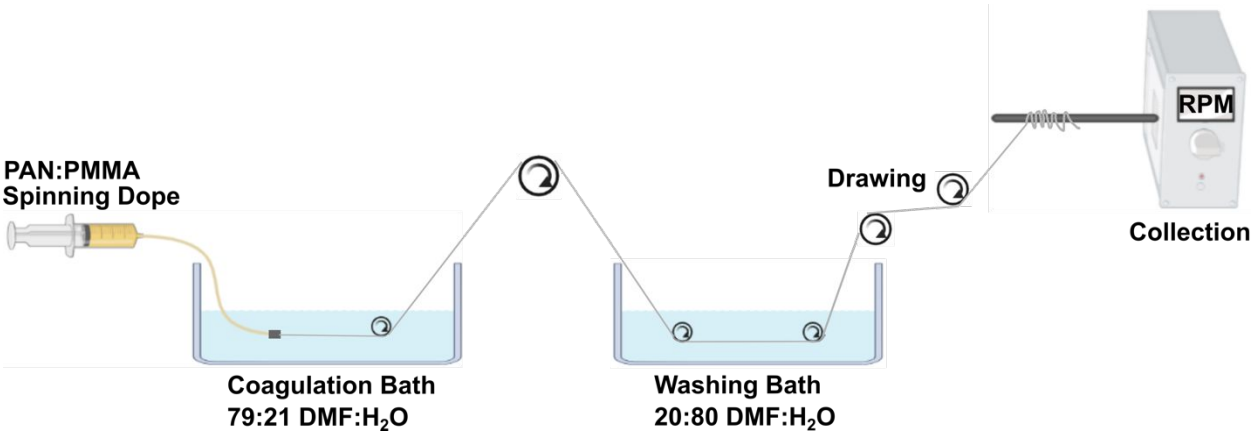

Figure 1. Schematic of in-house wet-spinning apparatus for synthesizing porous carbon microfibers. PAN/PMMA spinning dopes dissolved in DMF were extruded into a coagulation bath with continuous stretching and washed prior to collection to create controlled, nanoporous and microporous microfibers (Created in BioRender.com). See Supplemental Movie 1 for a movie of fiber formation.

Precursor, plasticized copolymer-derived microfibers were fabricated using the well-established technique of wet-spinning for fiber diameter uniformity and alignment.[14,17,18] Wet-spinning consisted of using a 20% w/w spinning dope of a mixture of polyacrylonitrile (PAN – the most common carbon fiber precursor) and poly(methyl methacrylate) (PMMA) dissolved in N,N-dimethyl formamide (DMF) (Figure 1). Fundamental polymer wet-spinning principles are used to achieve microfiber formation, as the spinning dope is injected into a coagulation bath of high solvent and low water concentrations.[14,17] The inherent concentration gradient between the solution dope and coagulation bath causes DMF to begin to diffuse from the precursor into the bath, allowing for plasticization to begin during the early stages of fiber formation. The diameter of the PAN/PMMA precursor fiber is ultimately dictated by the needle gauge size and stretching applied during the wetspinning process. This dictates the incident cross sectional area of the precursor solution coming into contact with the coagulation bath and controls the tension held on the plasticized fiber as solvent begins to diffuse from the precursor fiber, ultimately shrinking the diameter. Tension was maintained on the precursor fiber for continuous stretching as the fiber is transferred to a washing bath of low solvent and high water concentrations to further diffuse solvent from the precursor while reducing fiber diameter and preserving diameter uniformity. The

precursor is then collected for drying prior to heat treatment. A video of the in-house constructed wet-spinning setup can be seen in Supplemental Movie 1.

The PAN/PMMA copolymer precursor underwent published carbonization and annealing procedures[14,17] permitting carbon framework fabrication and PMMA sacrificial block decomposition[7,9,10,15,23] to generate highly roughened, macroporous microfibers. Fibers were first stabilized in air at 280°C followed by temperature ramping to 1,000°C under a N_2 atmosphere initiating carbonization while expelling PMMA and non-carbonaceous elements leaving macroporous geometries across the fiber's surface. Spinning dope compositional changes impact macroporous geometry uniformity across the microfiber, hindered greatly by the concentration of PMMA; thus, we characterized several fabricated microfibers with varying PMMA concentrations to analyze fiber pore uniformity. Heat-treatment procedures were succeeded by microfiber surface characterization and microelectrode fabrication for electrochemical characterization. We believe these fibers revolutionize the concept of local trapping of electroactive speciess for significantly improved detection capabilities by providing an entirely macroporous substrate with increased edge plane character for redox cycling capabilities.

Copolymer-derived porous carbon fiber surface characterization

Scanning Electron Microscopy. Scanning electron microscopy (SEM) was used to qualitatively analyze the morphology of the synthesized copolymer-derived porous carbon microfibers to investigate pore uniformity and size upon altering PMMA composition. Here, we investigated varied spinning dope copolymer concentrations from 95/5 to 70/30 PAN/PMMA assuming pore abundance increases as PMMA composition increases. Characterization of two of these microfibers (Figure 2) exhibit common striations seen on the surface of traditional CF with high degrees of visible surface roughness and large differences in pore abundance and uniformity. Interestingly, we observe large macro/micro pore sizes on all copolymer-derived fibers regardless of PMMA composition, differing from previous work investigating block-

copolymerization of PAN and PMMA to generate uniform nanoporosity with electrospinning.[22,24,25] Here, we report microfibers from 95/5 PAN/PMMA with a diameter of 74.4 ± 9.4 μm (n = 8) with pore widths of 350 ± 20 nm (Figure 2A n = 50 – in ImageJ, Table 1). Fibers of this diameter are known to cause tissue damage[26] and pore widths of this magnitude are too small to allow for effective local trapping of electroactive species. Previous work shows pores for local trapping are only effective for redox cycling at geometries on the diffusional scale of the analyte of interest.[6,27] Increasing the PMMA composition for microfibers to a spinning dope of 75/25 PAN/PMMA generates microfibers with a significantly smaller diameter of 21.18 ± 1.02 μm (Unpaired t-test, $p = 0.0001$, n = 8, Table 1) and significantly larger pore widths of 730 ± 50 nm (Unpaired t-test, $p < 0.0001$, n = 50, Table 1). Porous carbon microfibers (PCMFs) using 75/25 PAN:PMMA generated optimal fiber diameter, pore size, and relative pore uniformity (Figure 2B-C). These features are optimal for both biocompatibility (due to smaller size) and pore geometries compatible for local trapping. Local trapping occurs when pore geometries are on the diffusional scale of the analytes of interest (i.e. for dopamine = 0.9 μm).[6] Here, the pore size distribution observed on PCMFs are on the size-scale compatible for local trapping. We also would like to note that when increasing the PMMA composition to 30% w/w in 70/30 PAN/PMMA microfibers, the PMMA concentration exceeds its composition limit resulting in fiber integrity destruction upon heat treatment due to the combining of macropores throughout the fiber's framework (data not shown); thus, we chose 75/25 PAN:PMMA as optimal.

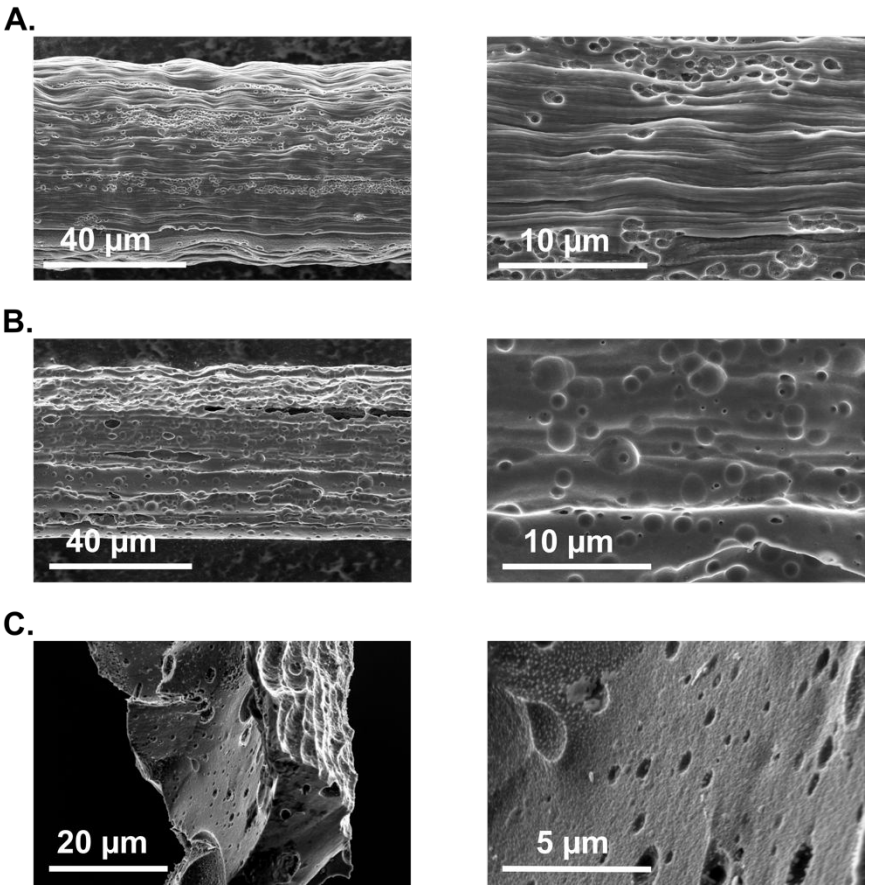

Figure 2. The weight percent of PMMA in the spinning dope impacts the uniformity and size of pores. Scanning electron microscopy images reveal low pore uniformity and small pore sizes at low PMMA compositions and high PMMA compositions leading to macropore sizes and improved uniformity. (A) 95/5 PAN/PMMA synthesized porous carbon fibers. (B) 75/25 PAN/PMMA synthesized porous carbon fibers. (C) Cross-sectional images of fiber tip of 75/25 PAN/PMMA synthesized porous carbon microfibers exhibit pores within the interior of the fiber. Scale bar on images.

Atomic Force Microscopy. Quantification of the average macropore size of PCMF with 25% w/w PMMA reveals pores on a dimensional scale comparable to the diffusion kinetics of neurotransmitters for local trapping. Atomic force microscopy (AFM) imaging was used to quantitatively analyze the surface topology of porous regions across several samples of PCMF as well as compare the porous topologies to that of traditional carbon fiber (CF). AFM provides accurate surface roughness measurements over a large PCMF area (2-4 μm scan), and denotes evident surface topology changes compared to CF (Figure 3). Surface roughness changes were accurately depicted by calculating the average maximum height across the image (R_z). Traditional

CF, known for its relatively smooth topology,[28] had a calculated average maximum roughness of 9.6 ± 1.9 nm (n = 5) which is comparable to previously reported values (Figure 3A).[29] AFM imaging of PCMF (the optimized macroporous microfiber described above) depicts circular macropores with an average R_z value of 730 ± 50 nm, which was significantly different from CF (Figure 3B and Table 1, Unpaired t-test, $p < 0.0001$, n = 6). The measured pores presented here are also different in size compared to traditionally electrospun block-copolymerized nanofibers[8,24,25] consisting of micropores of ~ 1 nm and mesopores of ~ 10 nm in diameter. Our reported pore sizes are dimensionally on the same scale as previously reported roughened carbon nanomaterials for local analyte trapping. Because of this, we hypothesized that our newly synthesized carbon-fibers would be capable of enhanced neurotransmitter detection by improvements in redox cycling capabilities and frequency independent behavior (explored later in this work). Pore geometries also provide an interactive environment during analyte desorption creating collision sites adding to local trapping. Depth profiles are presented as insets to depict depth fluctuations across the AFM height scans. We would like to note that the curvature of these microfibers leaves room for slight deviations in the quantified values reported but are accurate enough to make these pore size inferences. Also, AFM was not further used to characterize the surface structures of 95/5 PAN/PMMA fibers due to their inferior electrochemical properties (presented in a later section).

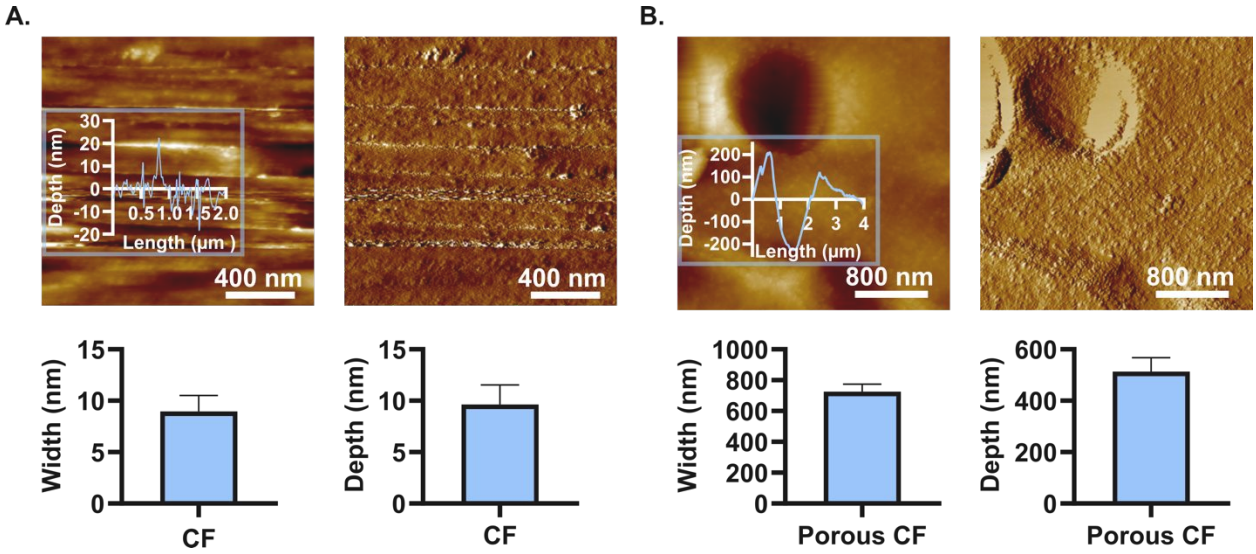

Figure 3. Atomic force microscopy (AFM) images reveal low surface roughness for traditional carbon fiber compared to large pore width and depth for 75/25 PAN/PMMA wet-spun porous carbon fibers. (A) Traditional carbon fiber has low roughness width (9.0 ± 1.5 nm) and roughness depth (9.6 ± 1.9 nm). Inset shows the depth of crevices across the CF surface over a 2 μm AFM scan with low roughness variability. (B) 75/25 PAN/PMMA wet-spun fibers exhibit both high pore width and depth of 730 ± 50 nm and 510 ± 50 nm, respectively. Inset shows the depth of pores across the porous CF surface over a 4 μm AFM scan with high depth fluctuations.

Tensile Strength and Tensiometry Analysis. Carbon fiber is a well-established working electrode material for bioanalysis due to its conductivity, oxide-rich nature, minimal size, and excellent mechanical properties. Here, we compare the extent to which a porous framework influences the mechanical properties of the fiber. First, we confirmed the high tensile strength values of 393.2 ± 98.0 ksi for traditional CF (Figure 4A), similar to previous reports.[30,31] Industrial synthesis and stretching mechanisms aid tensile properties immensely, but CF is also commonly coated in hydrosizing solutions to enhance strength-to-weight ratios for applications outside of chemical sensing. Our home-built wet-spinning stretching mechanisms, accompanied by no hydrosizing to ensure pore geometries are maintained, produce copolymer-based PCMFs with a tensile strength of only 28.5 ± 1.9 ksi (Figure 4A), a significant decrease from traditional CF (Unpaired t-test, p = 0.0205, n = 3, Table 1). Future work could focus on improving the mechanical properties of these porous microfibers.

The edge plane of carbon surfaces is well-known for its higher electron density and surface free energy enabling enhanced electrochemical activity, and we hypothesize that pore geometries should provide an increase in edge plane and defect sites on the carbon fiber surface. An abundance of edge-plane sites leads to highly hydrophilic surfaces; whereas, surfaces predominated by basal plane surfaces are more hydrophobic. Here, tensiometry measurements on a single fiber was done to measure the contact angle in water to determine the surface free energy. Tensiometry provides a means for investigating surface chemistry's influence over fiber wettability as opposed to surface roughness, giving insight into surface chemistry changes[32,33] at porous fibers. We show that PCMF's provide a near 2-fold increase in surface free energy compared to traditional CF (Figure 4B). Oxide functionalization of carbon fiber is predominately focused on the edge plane providing a more hydrophilic surface interaction, denoted by a reduced advancing contact angle. An advancing contact angle of 87.00 $\pm$ 1.62° was measured for traditional CF (similar to previous reports)[34], which is much more hydrophobic[35] than the contact angle measured on PCMFs (39.07 $\pm$ 2.21°). These differences in contact angle were statistically different from each other (Unpaired t-test, $p < 0.0001$, $n = 15$, Figure 4B and Table 1). Due to geometry and surface roughness' role in tensiometry measurements, the Wenzel contact angle correction equation[36] was used to understand the impact pores of 730 $\pm$ 50 nm width and 510 $\pm$ 50 nm height have on contact angle measurements. The area correction factor for the ratio of interfacial and projected area is as follows:

$$r = \frac{(Textured\ Surface\ Area) - (Cross\ Sectional\ Area)}{(Cross\ Sectional\ Area)} * 100\%$$

where *r* is the area factor, ***textured surface area*** is the surface area of a pore (assumed to be spherical with a diameter of 730 nm), and ***cross-sectional area*** is the surface area of a flat, circular region of the same diameter as the textured surface area. This ratio factor can then be applied to Wenzel's statement on the relationship of contact angle and surface roughness:

$$cos\Theta_m = rcos\Theta_Y$$

where $cos\Theta_m$ is the measured contact angle, $cos\Theta_Y$ is the corrected Young's contact angle, and a smooth surface has a ratio factor equal to 1 and roughened surfaces have r > 1. PCMF pore sizes produce a ratio factor of r = 1.01, and a minor ratio factor has a low impact on the advancing contact angle negligibly increasing the value to 39.80 ± 2.15° (Unpaired t-test, p = 0.9231, n = 15). Advancing contact angles are directly correlated to surface free energy values where we report an increase from 33.80 ± 1.85 mN/m for CF to 59.14 ± 2.77 mN/m for PCMF (Unpaired t-test, p = 0.0016, n=3, Figure 4B and Table 1). These surface free energy enhancements support that the surface chemistry of PCMF is vastly different from traditional CF with edge plane-dense regions across the entirety of these porous fibers.

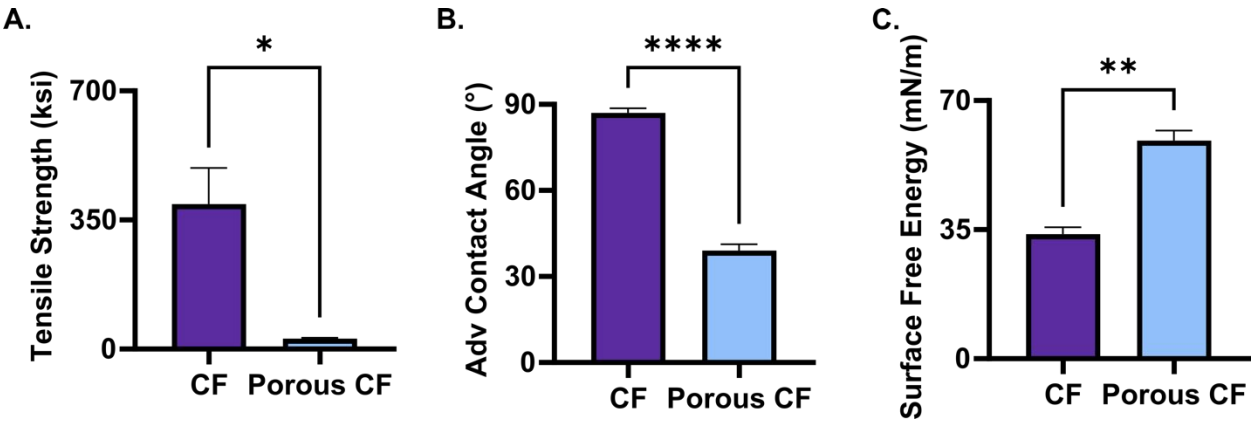

Figure 4. 75/25 PAN/PMMA porous microfibers exhibit lower tensile strength with increased surface free energy compared to traditional CF. (A) Traditional CF has a tensile strength of 393.2 ± 98.0 ksi while 75/25 PAN/PMMA porous microfibers have a tensile strength of 28.5 ± 1.9 ksi (Unpaired t-test, p = 0.0205, n = 3). (B) Traditional CF and 75/25 PAN/PMMA porous microfibers show a contact angle of 87.00 ± 1.62° and 39.07 ± 2.21°, respectively (Unpaired t-test, p < 0.0001, n = 15) and (C) a surface free energy of 33.80 ± 1.85 mN/m and 59.14 ± 2.77 mN/m, respectively (Unpaired t-test, p = 0.0016, n = 3).

Table 1. Fiber diameter, pore width/depth, tensile strength, and surface free energy of PAN/PMMA porous carbon fibers compared to traditional carbon fiber.

PAN/PMMA Composition	Fiber Diameter (μm)	Pore Width (nm)	Max Pore Height / R_z (nm)	Tensile Strength (ksi)	Surface Free Energy (mN/m)
95/5	74.40 ± 9.44	350 ± 20	----------	---------	----------
75/25	[a]21.18 ± 1.02***	[b]730 ± 50****	[c]510 ± 50****	[d]28.5 ± 1.9	[e]59.14 ± 2.77**
Traditional CF	7	----------	9.6 ± 1.9	393.2 ± 98.0*	33.80 ± 1.85

[a]Significant decrease in fiber diameter following increase in PMMA sacrificial block composition from 5% to 25% (Unpaired t-test, p = 0.0001, n = 8). [b]Significant increase in average pore size when increasing PMMA sacrificial block composition from 5% to 25% (Unpaired t-test, p < 0.0001, n = 50). [c]Significant increase in max pore height (R_z) in copolymer-based microfibers than traditional CF (Unpaired t-test, p < 0.0001 , n = 5-6). [d]Significant decrease in tensile strength from traditional CF to copolymer-based porous microfibers (Unpaired t-test, p = 0.0205, n = 3). [e]Significant increase in surface free energy using 75/25 PAN/PMMA porous microfibers (Unpaired t-test, p = 0.0016, n=3).

Raman Spectroscopy. Identification of the carbon structures present in a specific sample can be performed using Raman spectroscopy to characterize the carbon hybridization present.[37,38] CF is well-known as an amorphous carbonaceous material, but, despite its low degree of edge plane character and surface defects, has led the charge as the traditional working electrode for real-time neurotransmitter detection. Here, we hypothesized that pore structures should consist of higher edge plane character and defect sites for more sought-after electrochemical detection properties. We used Raman spectral mapping of traditional CF and PCMF to confirm this hypothesis by analyzing the sp^2 and sp^3 hybridization of these surfaces.[37,38] Of note, the diameter and curvature of these fibers resulted in two different dimensions used for map acquisition. Raman spectroscopy of carbon materials is commonly defined by two main bands: the D band (~1350 cm^{-1}) giving information on the surface oxidation and defect degree and the G band (~1580 cm^{-1}) directly correlated to the presence of graphitic carbon. By analyzing the ratio of the D and G band intensity (I_D/I_G), we characterized the degree of defects on the surface of PCMF as compared to traditional CF.[39–41] When assessing the disorder of a sample, it is well understood that these two bands are commonly the superposition of various bands, so peak fitting was used to represent the chemical makeup of these fiber structures more accurately. Peak fitting revealed five bands present from 1000 – 1800 cm^{-1}: D, G, D* (~1150 – 1200 cm^{-1}), and D' (~1615 – 1635 cm^{-1}) (Figure S1). The resulting I_D/I_G 3-dimensional ratio intensity maps are plotted in Figure 5.[42,43]

Critical assessment of traditional CF and synthesized PCMF reveals increases in the disorder degree and edge plane character at porous microfibers. Traditional CF (Figure 5A) had

a low, but uniform, I_D/I_G across the length of the fiber (~1.23). This result was expected and implies a relatively low degree of disorder and edge plane character along the length of the carbon fiber. These properties drastically changed for the map of PCMF (Figure 5B). Interpreting this map provides a chemical, "topographical" analysis of the PCMF surface where we observe that the minimum I_D/I_G intensity ratios are greater than the maximum disorder degrees measured on the traditional CF. We also observe edge plane/defected "hotspots" visualized as spikes in the Raman map with I_D/I_G > 2.000. The Raman map provides topographical and chemical information supporting our hypothesis that pore sites produce abundant edge plane character with high surface defects and disorder. These hotspot spikes in the PCMF Raman map denotes the presence of pores across the fiber's surface with greater basal plane contributions outside of the pore structures. This structural, macroporous framework could provide the key to generating highly attractive carbon surfaces for electrochemical sensing applications with relative ease at the forefront of carbon fiber syntheses. We present a means to maximize edge plane site abundance with macropore geometries across the entire sensing surface.

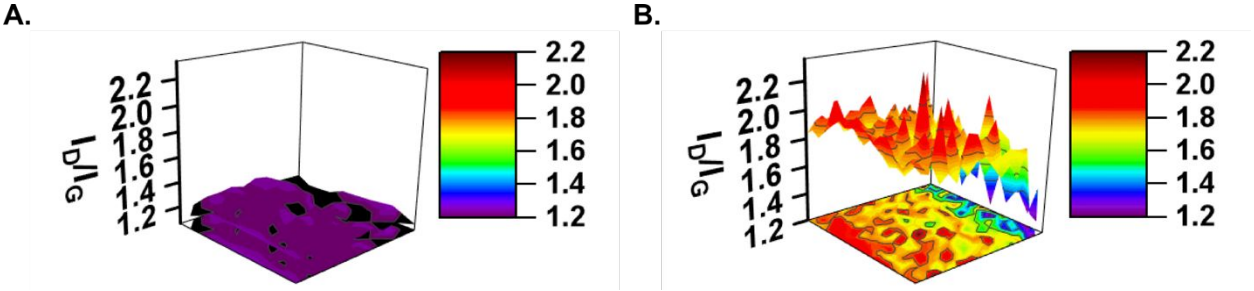

Figure 5. Raman spectroscopy mapping shows enhancements in D/G ratio within pore structures of 75/25 PAN/PMMA synthesized porous fibers exhibiting high edge plane character and high surface defects, whereas traditional CF shows uniform, low D/G ratio across its surface. (A) 2 μm x 2 μm, 3-dimensional Raman spectroscopy map of traditional CF. (B) 10 μm x 10 μm, 3-dimensional Raman spectroscopy map of 75/25 PAN/PMMA synthesized fiber.

PCMF electrochemical analysis with fast-scan cyclic voltammetry

75/25 PAN/PMMA PCMFs were selected from all copolymer fibers not only for their superior edge plane character and pore uniformity, but for the electrochemical enhancements they provide to neurotransmitter detection. Here, fast-scan cyclic voltammetry (FSCV) was used

to electrochemically characterize porous microfibers because it is a prominent technique used for real-time analysis of electroactive neurotransmitters. Dopamine was used as the test analyte because its electrochemical properties are well characterized with FSCV. Electrochemical characterization of PCMF with FSCV shows significant impacts to dopamine interaction at the electrode surface. We provide evidence that the macroporous geometries play a prominent role in enhanced oxidation current and, most notably, redox cycling (Figure 6). Altering the foundational polymer makeup of these precursor fibers provides macropore sites across the entirety of the sensing surface to reevaluate this redox cycling phenomena for FSCV analysis, providing a pseudo thin layer cell type environment.[44,45] This is evident in the background-subtracted cyclic voltammogram (CV) in Figure 6 for 1 μM dopamine. The degree of redox cycling (ι_{ox}/ι_{red}) is determined by the ratio of oxidation to reduction current where perfect redox reversibility gives a ratio of 1.0. A typical redox cycling ratio for traditional CF is ~2.0[22] due to the desorption properties of dopamine's oxidized partner, dopamine-*o*-quinone (DOQ). Here, we show a redox cycling ratio approaching nearly reversible processes with a ratio of ι_{ox}/ι_{red} = 1.3 ± 0.1 (Figure 6B, Table 2, n = 8). We speculate that this is due to local trapping of DOQ within macropores depleting the quantity of reduction product loss following diffusion processes. These porous geometries also provide some electrocatalytic properties by enhancing the electron transfer kinetics of dopamine at these surfaces, reducing oxidation/reduction peak splitting to 0.95 ± 0.03 V. This concept is common with pores on the nanoscale, so we believe the distribution of pore sizes present in PCMF proves feasibility for kinetic improvements additional to redox improvements. Notably, PCMF microelectrodes exhibit stable capacitive behavior with maintained capacitive current of 2480 ± 300 nA, comparable to previous traditional CF work[22] (Figure 6C, n = 8). The surface area of PCMF is increased by the pore geometries present, but the resulting capacitive current increases can be combatted by reducing working electrode lengths. Capacitive current also remains unchanged when analyzing multiple injections of TRIS buffer (Figure 6D). This result

provides evidence that these electrodes are stable at rapid scan rates over time enabling accurate background substraction for FSCV analysis. Not only is the result important for FSCV, but it also provides evidence that the capacitance is stable and large, a potentially important characteristic for energy storage applications.

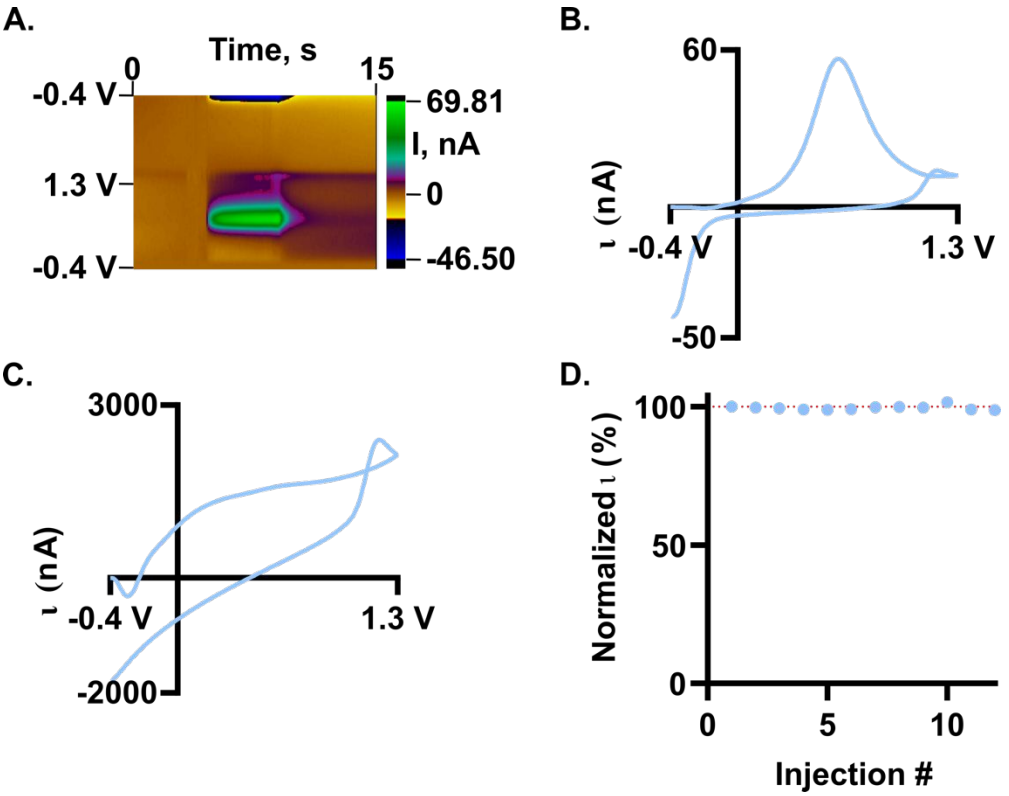

Figure 6. PAN/PMMA-derived porous carbon fibers exhibit high oxidative current due to increased edge plane surface area within porous geometries allowing for major improvements in redox cycling (i_{ox}/i_{red}) with a stable, non-appreciable increases in background current (A) Example false color for 1 μM dopamine detected at PAN/PMMA porous carbon fiber microelectrode. and (B) Corresponding background subtracted CV showing redox cycling enhancements of i_{ox}/i_{red} = 1.3 ± 0.1 (n = 8) and (C) background capacitive current CV (n = 8). (D) Background current over 12-repeated injections of TRIS buffer indicating stability with no fluctuations in capacitive current with a total drop in capacitive current of only 1.3 ± 1.1 %.

Electrochemical enhancements to catecholamine detection with PCMF

The improved redox cycling and surface area increases observed for PCMF microelectrodes ultimately enhanced dopamine detection sensitivity. We observed an over two-fold increase in sensitivity compared to traditional CF, which we speculate is attributed to increased adsorption sites produced by porous geometries.[22] Concentrations from 0.250 to 300

μM were tested to determine the sensitivity and limit of detection (LOD) of dopamine using PCMF (Figure 7, n = 10). Analysis of the current profile over this concentration range shows common linearity at low concentrations with saturation occurring at high concentrations (Figure 7A), comparable to traditional CF saturating at concentrations > 10 μM. Interestingly, PCMF's high edge plane character and pore site-rich surface area with increased adsorption interaction regions achieves saturation at concentrations > 40 μM, increasing the linear working region 4-fold (Figure S2, R^2 = 0.8718, n = 10). Analyzing the traditional CF linear working region of 0-10 μM (Figure 7B) generates a sensitivity of 16.9 ± 0.8 nA/μM (Table 2, R^2 = 0.8520). We would like to note that lower R^2 linearity coefficients are impacted by slight variability in fiber diameters due to in-house wetspinning stretching and alignment mechanisms compared to industrial setups. LOD analysis was calculated as three times the standard deviation of the noise at the lowest concentration tested (0.250 μM, Figure 7C, ι_{ox}/ι_{red} = 1.3), and was determined to be 0.6 ± 0.2 nM (Table 2) . This LOD is vastly improved from that of traditional CF, where the average LOD is reported in the range of 10-15 nM.[22]

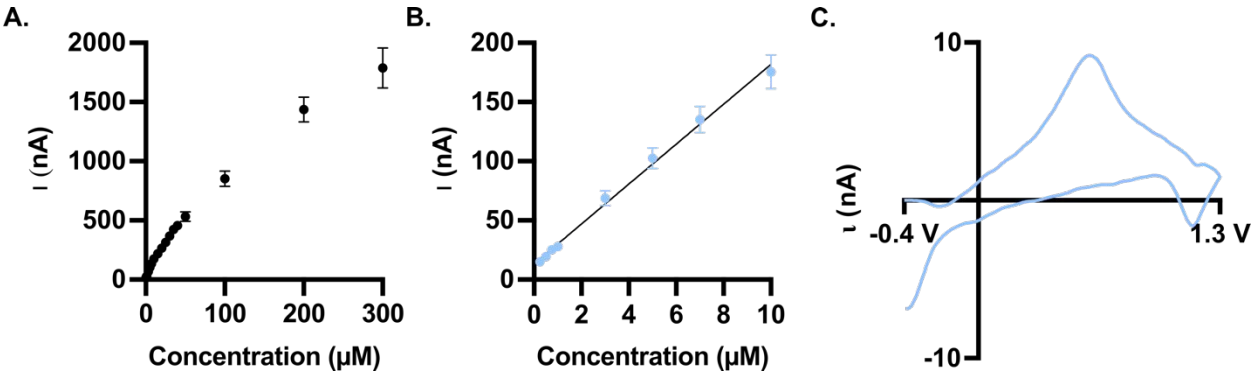

Figure 7. 75/25 PAN/PMMA porous CF provide enhanced detection sensitivity to dopamine while extending the traditional linear working region from 10 to 40 μM and improved sensitivity to dopamine compared to traditional CFME (n = 10). (A) Full concentration curve of 75/25 PAN/PMMA porous CF showing saturation at concentrations > 40 μM. (B) Concentration curve spanning from 0.25 – 10 μM shows a sensitivity of 16.9 ± 0.8 nA/μM (R^2 = 0.8520). (C) Background subtracted CV of 250 nM DA using 75/25 PAN/PMMA porous CF.

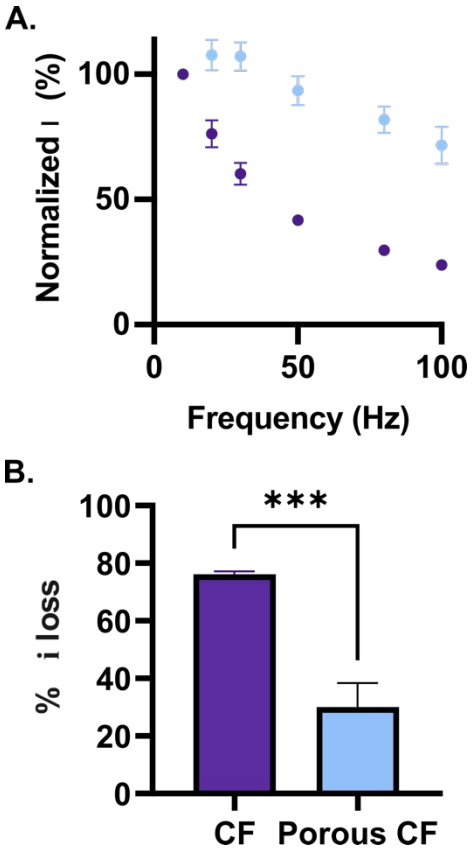

Figure 8. Analysis of the effect of scan repetition frequency has on the redox interaction of dopamine at traditional and 75/25 PAN/PMMA porous CF shows local trapping occurring at porous fibers provides redox cycling allowing for greater frequency independence for higher temporal resolution. (A) Normalized peak oxidative current analysis of 1 μM dopamine at traditional (purple) and 75/25 PAN/PMMA porous (light blue) CF. (B) Analysis of frequency independence denoted by the percent of normalized peak oxidative current lost at a scan repetition frequency of 100 Hz compared to 10 Hz for traditional (purple) and 75/25 PAN/PMMA porous (light blue) CF losing 76.2 ± 1.0 and 30.1 ± 8.3 (Unpaired t-test, $p = 0.0003$, $n = 6$).

High waveform application frequency measurements are capable on PCMF microelectrodes with FSCV. Increases in application frequency are known to decrease the analyte pre-accumulation time at the surface of the microelectrode. Previous reports have acknowledged that pore local trapping is a common avenue to move toward more frequency independence ultimately improving the temporal resolution.[5,16] To test for frequency independence, we analyzed the extent to which dopamine's oxidation current changes as a function of waveform application frequency (Figure 8). Traditionally, FSCV uses a waveform application frequency of 10 Hz with a pre-concentration time of 91.5 ms at the applied holding potential of -0.4 V. We can analyze how

decreasing preconcentration time impacts analyte surface concentration prior to waveform application by increasing the application frequency, normalizing oxidation current to the current achieved at 10 Hz, and plotting this normalized current versus application frequency. Using a CFME, we observe a steady decrease in oxidation current with increased frequency (Figure 8A). At application frequencies of 100 Hz, the time to preconcentrate the electrode is reduced to 1.5 ms and only 23.8 $\pm$ 1.0 % of the oxidation current is maintained (Figure 8B). Similar to redox cycling degree, this current loss as a function of frequency can be used to determine the reversibility of a redox reaction impacted by the macropore geometries present within PCMF. Based on prior reports describing local trapping of dopamine on roughened electrode surfaces, the macropores of PCMF should also show improved frequency independence. Although oxidation current is decreased as applied frequency is increased, oxidation current is maintained up to a frequency of 30 Hz for PCMF. Following 30 Hz, we observe a small decrease in oxidation current as the applied frequency is increased to 100 Hz (Figure 8A). Local trapping and increased frequency independent behavior of PCMF results in only a 30.1 $\pm$ 8.0% normalized current loss, which is a significant improvement over traditional CF (Figure 8, Table 2, unpaired t-test, $p = 0.0003$, $n = 6$). At a traditional CFME, dopamine adsorbs to the electrode surface nearly 10× as much as dopamine-o-quinone (DOQ) rendering smaller reduction peaks than oxidation peaks. We speculate that not only is DA trapped in the pores but that DOQ may also interact more strongly at the pores compared to traditional CFME's leading to more enhanced local trapping and ultimately more frequency independent behavior. Although PCMFs provide more uniform pore coverage across the carbon microfiber's surface, a lack of true frequency independence is observed, unlike what has been observed on roughened carbon nanomaterials like carbon nanotube fibers and nanospikes.[29,46] We believe this is associated with the pore-free regions of the fiber and also the pore size distribution resulting in the formation of smaller pores than the macropore size required for local trapping. Additionally,

our results may indicate that absolute frequency independence could be dependent on not only electrode geometry, but also the surface reactivity. All prior studies demonstrating frequency independence with FSCV have been on carbon nanomaterials vs. here, we demonstrate this phenomena on carbon-fiber. Although absolute frequency independence is not achieved like previous reports on CNT-based materials,[5,16] we observed a significant improvement in redox cycling and frequency independence from previous CF porous material modifications[22] showing the impact of an entirely porous substrate used as a biosensing material. The improved temporal resolution of PCMF will ultimately enable more rapid detection of neurotransmitters when implanted as a biosensor.

Table 2. Electrochemical characterization summary of oxidation to reduction current ratio, electron transfer kinetics, capacitive current, average sensitivity, LOD, and frequency dependence for traditional carbon fiber and 75/25 PAN/PMMA porous CF.

	i_{ox}/i_{red}	ΔE_p	i_c (nA)	Sensitivity (nA μM^{-1})	Limit of Detection (nM)	Percent Current Loss (%)
CF	[22]2.1 ± 0.2	[22]1.01 ± 0.01	[22]2430 ± 140	[22]6.9 ± 0.4	[22]6.7 ± 1.0	76.2 ± 1.0
Porous CF	1.3 ± 0.1	0.95 ± 0.03	2480 ± 300	16.9 ± 0.8	0.6 ± 0.2	[a]30.1 ± 8.3***

[a]Significant decrease in the percent of current lost when changing the scan acquisition frequency from 10 Hz to 100 Hz (unpaired t-test, p = 0.0003, n = 6).

We show the extent to which porous geometries impact real-time detection of different classes of neurotransmitters. A key neurotransmitter class of interest that remains difficult to detect are the purines. The two purines tested here undergo a multi-step oxidation scheme. Adenosine undergoes three 2 electron/2 proton oxidation; whereas, guanosine undergoes two 2 electron/2 proton reactions. In FSCV, it is well established that detection of the secondary oxidation and tertiary oxidation product (for adenosine) is more difficult than capturing the primary oxidation reaction.[47–50] Analysis of adenosine and guanosine (Figure S3 C,D) not only show enhanced primary oxidation current at PCMF's but also we observe increases in conversion of primary oxidation product to secondary oxidation product. We speculate that this improvement in

the ratio of secondary to primary peak is a result of local trapping of the purine in the pores, further catalyzing the oxidation reaction. Improvements in detection of all the oxidation peaks for the purines can aid in improvements in selectivity by creating a more identifiable “fingerprint” for in-tissue analysis. We also tested the indolamine neurotransmitter class, which includes both serotonin and melatonin (Figure S3, F). For melatonin, we observe an increase in the presence of it’s well-characterized side electropolymerization peaks.[51] This result demonstrates that pores may actually be detrimental for detection of analytes that are known to electropolymerize and foul the electrode surface. Overall, these results indicate that precise tailoring of the electrode surface is necessary for enhancing specific analytes of interest.

Conclusion

Wetspinning has held a tight grasp on traditional carbon fiber production for fiber uniformity and tensile properties, but amorphous carbon fiber lacks necessary surface morphology and edge plane abundance for attractive, real-time electrochemical neurochemical detection. By adding a secondary copolymer to the wetspinning precursor dope, we present a novel method for fabricating relatively uniform, macroporous carbon microfibers of enhanced edge plane character denoted by highly concentrated defect-rich pores. To date, past work has focused on carbon fiber surface modifications for pore enhancements or the use of carbon nanomaterials. We present a brand new material for electrochemical detection which overcomes the need for cumbersome carbon-fiber modification while still enabling the use of carbon fiber. Here, we show that copolymer wet-spining methods generate PCMF macroporous geometries of high edge plane character suitable for local trapping to improve electrochemical redox cycling, temporal resolution, and measurement sensitivity while enhancing carbon fiber surface free energy. We anticipate that these porous microfibers could be useful for several applications beyond neurochemical sensing including supercapaciters, energy storage, among others.

Supporting Information

We provide a procedural video and experiments to support our manuscript claims. The wetspinning processing apparatus video shows the in-house apparatus and setup constructed for all porous carbon microfiber precursor fiber formation. Analysis of current vs. concentration at greater concentrations than traditional linear range data supports saturation at great concentrations than traditional CF. Lastly, overlayed cyclic voltammograms of neurotransmitters other than dopamine detected at both traditional CF and porous carbon microfibers are present to compare analyte interactions at differing geometries.

Conflicts of Interest

The authors declare no conflicts of interest.

Acknowledgements

The research reported in this manuscript was supported by the National Institute of Allergy and Infection Diseases of the National Institutes of Health under Award Number R01AI151552, the National Science Foundation under Award Number 2143520, and the Alfred P. Sloan Foundation. The content is solely the responsibility of the authors and does not necessarily represent the official views of the NIH, NSF, or Alfred P. Sloan Foundation. The authors would also like to thank Prof. Noe Alavarez and Abdul Hoque at the University of Cincinnati for acquiring atomic force micrographs/images.

References

(1) Bath, B. D.; Michael, D. J.; Trafton, B. J.; Joseph, J. D.; Runnels, P. L.; Wightman, R. M. Subsecond Adsorption and Desorption of Dopamine at Carbon-Fiber Microelectrodes. *Anal. Chem.* **2000**, *72* (24), 5994–6002. https://doi.org/10.1021/ac000849y.

(2) Zachek, M. K.; Hermans, A.; Wightman, R. M.; McCarty, G. S. Electrochemical Dopamine Detection: Comparing Gold and Carbon Fiber Microelectrodes Using Background Subtracted Fast Scan Cyclic Voltammetry. *J Electroanal Chem (Lausanne Switz)* **2008**, *614* (1–2), 113–120. https://doi.org/10.1016/j.jelechem.2007.11.007.

(3) McCreery, R. L. Advanced Carbon Electrode Materials for Molecular Electrochemistry. *Chem. Rev.* **2008**, *108* (7), 2646–2687. https://doi.org/10.1021/cr068076m.

(4) McCreery, R. L.; Cline, K. K.; McDermott, C. A.; McDermott, M. T. Control of Reactivity at Carbon Electrode Surfaces. *Colloids and Surfaces A: Physicochemical and Engineering Aspects* **1994**, *93*, 211–219. https://doi.org/10.1016/0927-7757(94)02899-0.

(5) Cao, Q.; Shao, Z.; Hensley, D. K.; Lavrik, N. V.; Venton, B. J. Influence of Geometry on Thin Layer and Diffusion Processes at Carbon Electrodes. *Langmuir* **2021**, *37* (8), 2667–2676. https://doi.org/10.1021/acs.langmuir.0c03315.
(6) Shao, Z.; Puthongkham, P.; Hu, K.; Jia, R.; Mirkin, M. V.; Venton, B. J. Thin Layer Cell Behavior of CNT Yarn and Cavity Carbon Nanopipette Electrodes: Effect on Catecholamine Detection. *Electrochimica Acta* **2020**, *361*, 137032. https://doi.org/10.1016/j.electacta.2020.137032.
(7) Zhou, Z.; Liu, T.; Khan, A. U.; Liu, G. Block Copolymer–Based Porous Carbon Fibers. *Science Advances* **2019**, *5* (2), eaau6852. https://doi.org/10.1126/sciadv.aau6852.
(8) Li, C.; Li, Q.; Kaneti, Y. V.; Hou, D.; Yamauchi, Y.; Mai, Y. Self-Assembly of Block Copolymers towards Mesoporous Materials for Energy Storage and Conversion Systems. *Chem. Soc. Rev.* **2020**, *49* (14), 4681–4736. https://doi.org/10.1039/D0CS00021C.
(9) Thanh Nguyen, C.; Kim, D.-P. Direct Preparation of Mesoporous Carbon by Pyrolysis of Poly(Acrylonitrile- b -Methylmethacrylate) Diblock Copolymer. *Journal of Materials Chemistry* **2011**, *21* (37), 14226–14230. https://doi.org/10.1039/C1JM10920K.
(10) Yan, K.; Kong, L.-B.; Dai, Y.-H.; Shi, M.; Shen, K.-W.; Hu, B.; Luo, Y.-C.; Kang, L. Design and Preparation of Highly Structure-Controllable Mesoporous Carbons at the Molecular Level and Their Application as Electrode Materials for Supercapacitors. *J. Mater. Chem. A* **2015**, *3* (45), 22781–22793. https://doi.org/10.1039/C5TA05947J.
(11) Zander, N. E.; Strawhecker, K. E.; Orlicki, J. A.; Rawlett, A. M.; Beebe, T. P. Coaxial Electrospun Poly(Methyl Methacrylate)–Polyacrylonitrile Nanofibers: Atomic Force Microscopy and Compositional Characterization. *J. Phys. Chem. B* **2011**, *115* (43), 12441–12447. https://doi.org/10.1021/jp205577r.
(12) Kim, C.; Jeong, Y. I.; Ngoc, B. T. N.; Yang, K. S.; Kojima, M.; Kim, Y. A.; Endo, M.; Lee, J.-W. Synthesis and Characterization of Porous Carbon Nanofibers with Hollow Cores Through the Thermal Treatment of Electrospun Copolymeric Nanofiber Webs. *Small* **2007**, *3* (1), 91–95. https://doi.org/10.1002/smll.200600243.
(13) Alarifi, I. M.; Khan, W. S.; Asmatulu, R. Synthesis of Electrospun Polyacrylonitrile-Derived Carbon Fibers and Comparison of Properties with Bulk Form. *PLoS One* **2018**, *13* (8), e0201345. https://doi.org/10.1371/journal.pone.0201345.
(14) Morris, E. A.; Weisenberger, M. C. Solution Spinning of PAN-Based Polymers for Carbon Fiber Precursors. In *ACS Symposium Series*; Naskar, A. K., Hoffman, W. P., Eds.; American Chemical Society: Washington, DC, 2014; Vol. 1173, pp 189–213. https://doi.org/10.1021/bk-2014-1173.ch009.
(15) Hillmyer, M. Block Copolymer Synthesis. *Current Opinion in Solid State and Materials Science* **1999**, *4* (6), 559–564. https://doi.org/10.1016/S1359-0286(00)00006-1.
(16) Yang, C.; Hu, K.; Wang, D.; Zubi, Y.; Lee, S. T.; Puthongkham, P.; Mirkin, M. V.; Venton, B. J. Cavity Carbon-Nanopipette Electrodes for Dopamine Detection. *Anal. Chem.* **2019**, *91* (7), 4618–4624. https://doi.org/10.1021/acs.analchem.8b05885.
(17) Kaur, J.; Millington, K.; Smith, S. Producing High-Quality Precursor Polymer and Fibers to Achieve Theoretical Strength in Carbon Fibers: A Review. *Journal of Applied Polymer Science* **2016**, *133* (38). https://doi.org/10.1002/app.43963.

(18) Morris, E.; Weisenberger, M.; Rice, G. Properties of PAN Fibers Solution Spun into a Chilled Coagulation Bath at High Solvent Compositions. *Fibers* **2015**, *3* (4). https://doi.org/10.3390/fib3040560.

(19) Samimi, E.; Abolhasani, M. M.; Arbab, S. Producing Porous Polyacrylonitrile Fibers Using Wet-Spinning Method for Making Carbon Fibers. In *Eco-friendly and Smart Polymer Systems*; Mirzadeh, H., Katbab, A. A., Eds.; Springer International Publishing: Cham, 2020; pp 577–580. https://doi.org/10.1007/978-3-030-45085-4_139.

(20) Hu, W.; Xiang, R.; Zhang, K.; Xu, Q.; Liu, Y.; Jing, Y.; Zhang, J.; Hu, X.; Zheng, Y.; Jin, Y.; Yang, X.; Lu, C. Electrochemical Performance of Coaxially Wet-Spun Hierarchically Porous Lignin-Based Carbon/Graphene Fiber Electrodes for Flexible Supercapacitors. *ACS Appl. Energy Mater.* **2021**, *4* (9), 9077–9089. https://doi.org/10.1021/acsaem.1c01379.

(21) Chien, A.-T.; Liu, H. C.; Newcomb, B. A.; Xiang, C.; Tour, J. M.; Kumar, S. Polyacrylonitrile Fibers Containing Graphene Oxide Nanoribbons. *ACS Appl. Mater. Interfaces* **2015**, *7* (9), 5281–5288. https://doi.org/10.1021/am508594p.

(22) Ostertag, B. J.; Cryan, M. T.; Serrano, J. M.; Liu, G.; Ross, A. E. Porous Carbon Nanofiber-Modified Carbon Fiber Microelectrodes for Dopamine Detection. *ACS Appl. Nano Mater.* **2022**, *5* (2), 2241–2249. https://doi.org/10.1021/acsanm.1c03933.

(23) Nikolaidis, A. K.; Achilias, D. S. Thermal Degradation Kinetics and Viscoelastic Behavior of Poly(Methyl Methacrylate)/Organomodified Montmorillonite Nanocomposites Prepared via In Situ Bulk Radical Polymerization. *Polymers (Basel)* **2018**, *10* (5), 491. https://doi.org/10.3390/polym10050491.

(24) Liu, T.; Zhou, Z.; Guo, Y.; Guo, D.; Liu, G. Block Copolymer Derived Uniform Mesopores Enable Ultrafast Electron and Ion Transport at High Mass Loadings. *Nature Communications* **2019**, *10* (1), 675. https://doi.org/10.1038/s41467-019-08644-w.

(25) Serrano, J. M.; Liu, T.; Khan, A. U.; Botset, B.; Stovall, B. J.; Xu, Z.; Guo, D.; Cao, K.; Hao, X.; Cheng, S.; Liu, G. Composition Design of Block Copolymers for Porous Carbon Fibers. *Chem. Mater.* **2019**, *31* (21), 8898–8907. https://doi.org/10.1021/acs.chemmater.9b02918.

(26) Jaquins-Gerstl, A.; Michael, A. C. Comparison of the Brain Penetration Injury Associated with Microdialysis and Voltammetry. *J Neurosci Methods* **2009**, *183* (2), 127–135. https://doi.org/10.1016/j.jneumeth.2009.06.023.

(27) Cao, Q.; Puthongkham, P.; Venton, B. J. Review: New Insights into Optimizing Chemical and 3D Surface Structures of Carbon Electrodes for Neurotransmitter Detection. *Anal. Methods* **2019**, *11* (3), 247–261. https://doi.org/10.1039/C8AY02472C.

(28) Dilsiz, N. Plasma Surface Modification of Carbon Fibers: A Review. *Journal of Adhesion Science and Technology* **2000**, *14* (7), 975–987. https://doi.org/10.1163/156856100743013.

(29) Schmidt, A. C.; Wang, X.; Zhu, Y.; Sombers, L. A. Carbon Nanotube Yarn Electrodes for Enhanced Detection of Neurotransmitter Dynamics in Live Brain Tissue. *ACS Nano* **2013**, *7* (9), 7864–7873. https://doi.org/10.1021/nn402857u.

(30) Tran, N. T.; Patterson, B. A.; Kolodziejczyk, A. G.; Wu, V. M.; Knorr, D. B. Jr. Electrochemical Surface Treatment of Discontinuous Carbon Fibers. *Langmuir* **2019**, *35* (38), 12374–12388. https://doi.org/10.1021/acs.langmuir.9b01850.

(31) Karakassides, A.; Ganguly, A.; Tsirka, K.; Paipetis, A. S.; Papakonstantinou, P. Radially Grown Graphene Nanoflakes on Carbon Fibers as Reinforcing Interface for Polymer

Composites. *ACS Appl. Nano Mater.* **2020**, *3* (3), 2402–2413. https://doi.org/10.1021/acsanm.9b02536.

(32) Qiu, S.; Fuentes, C. A.; Zhang, D.; Van Vuure, A. W.; Seveno, D. Wettability of a Single Carbon Fiber. *Langmuir* **2016**, *32* (38), 9697–9705. https://doi.org/10.1021/acs.langmuir.6b02072.

(33) Lu, C.; Wang, J.; Lu, X.; Zheng, T.; Liu, Y.; Wang, X.; Zhang, D.; Seveno, D. Wettability and Interfacial Properties of Carbon Fiber and Poly(Ether Ether Ketone) Fiber Hybrid Composite. *ACS Appl. Mater. Interfaces* **2019**, *11* (34), 31520–31531. https://doi.org/10.1021/acsami.9b09735.

(34) Fu, X.; Lu, W.; Chung, D. D. L. Ozone Treatment of Carbon Fiber for Reinforcing Cement. *Carbon* **1998**, *36* (9), 1337–1345. https://doi.org/10.1016/S0008-6223(98)00115-8.

(35) GmbH, K. Wettability of Carbon Fibers Using Single-Fiber Contact Angle Measurements – a Feasibility Study. 3.

(36) Laurén, S.; Scientific, B. The Attension Theta Flex Optical Tensiometer with 3D Topography Module. 6.

(37) Wu, J.-B.; Lin, M.-L.; Cong, X.; Liu, H.-N.; Tan, P.-H. Raman Spectroscopy of Graphene-Based Materials and Its Applications in Related Devices. *Chemical Society Reviews* **2018**, *47* (5), 1822–1873. https://doi.org/10.1039/C6CS00915H.

(38) Ferrari, A. C.; Basko, D. M. Raman Spectroscopy as a Versatile Tool for Studying the Properties of Graphene. *Nature Nanotech* **2013**, *8* (4), 235–246. https://doi.org/10.1038/nnano.2013.46.

(39) Li, Y.; Jarosova, R.; Weese-Myers, M. E.; Ross, A. E. Graphene-Fiber Microelectrodes for Ultrasensitive Neurochemical Detection. *Anal. Chem.* **2022**, *94* (11), 4803–4812. https://doi.org/10.1021/acs.analchem.1c05637.

(40) Li, Y.; M. Fleischer, C.; E. Ross, A. High Young's Modulus Carbon Fibers Are Fouling Resistant with Fast-Scan Cyclic Voltammetry. *Chemical Communications* **2020**, *56* (58), 8023–8026. https://doi.org/10.1039/D0CC02517H.

(41) Syeed, A. J.; Li, Y.; Ostertag, B. J.; Brown, J. W.; Ross, A. E. Nanostructured Carbon-Fiber Surfaces for Improved Neurochemical Detection. *Faraday Discuss.* **2021**. https://doi.org/10.1039/D1FD00049G.

(42) King, A. A. K.; Davies, B. R.; Noorbehesht, N.; Newman, P.; Church, T. L.; Harris, A. T.; Razal, J. M.; Minett, A. I. A New Raman Metric for the Characterisation of Graphene Oxide and Its Derivatives. *Sci Rep* **2016**, *6* (1), 19491. https://doi.org/10.1038/srep19491.

(43) Claramunt, S.; Varea, A.; López-Díaz, D.; Velázquez, M. M.; Cornet, A.; Cirera, A. The Importance of Interbands on the Interpretation of the Raman Spectrum of Graphene Oxide. *J. Phys. Chem. C* **2015**, *119* (18), 10123–10129. https://doi.org/10.1021/acs.jpcc.5b01590.

(44) Venton, B. J.; Cao, Q. Fundamentals of Fast-Scan Cyclic Voltammetry for Dopamine Detection. *Analyst* **2020**, *145* (4), 1158–1168. https://doi.org/10.1039/C9AN01586H.

(45) Roberts, J. G.; Sombers, L. A. Fast-Scan Cyclic Voltammetry: Chemical Sensing in the Brain and Beyond. *Anal. Chem.* **2018**, *90* (1), 490–504. https://doi.org/10.1021/acs.analchem.7b04732.

(46) Cao, Q.; Hensley, D. K.; Lavrik, N. V.; Venton, B. J. Carbon Nanospikes Have Better Electrochemical Properties than Carbon Nanotubes Due to Greater Surface Roughness and Defect Sites. *Carbon* **2019**, *155*, 250–257. https://doi.org/10.1016/j.carbon.2019.08.064.

(47) Cryan, M. T.; Ross, A. E. Subsecond Detection of Guanosine Using Fast-Scan Cyclic Voltammetry. *Analyst* **2018**, *144* (1), 249–257. https://doi.org/10.1039/C8AN01547C.
(48) Swamy, B. E. K.; Venton, B. J. Subsecond Detection of Physiological Adenosine Concentrations Using Fast-Scan Cyclic Voltammetry. *Anal Chem* **2007**, *79* (2), 744–750. https://doi.org/10.1021/ac061820i.
(49) Li, Y.; Keller, A. L.; Cryan, M. T.; Ross, A. E. Metal Nanoparticle Modified Carbon-Fiber Microelectrodes Enhance Adenosine Triphosphate Surface Interactions with Fast-Scan Cyclic Voltammetry. *ACS Meas. Au* **2022**, *2* (2), 96–105. https://doi.org/10.1021/acsmeasuresciau.1c00026.
(50) Keller, A. L.; Quarin, S. M.; Strobbia, P.; Ross, A. E. Platinum Nanoparticle Size and Density Impacts Purine Electrochemistry with Fast-Scan Cyclic Voltammetry. *J. Electrochem. Soc.* **2022**, *169* (4), 046514. https://doi.org/10.1149/1945-7111/ac65bc.
(51) Hensley, A. L.; Colley, A. R.; Ross, A. E. Real-Time Detection of Melatonin Using Fast-Scan Cyclic Voltammetry. *Anal. Chem.* **2018**, *90* (14), 8642–8650. https://doi.org/10.1021/acs.analchem.8b01976.

Graphical Abstract